Published in final edited form as:

J Magn Reson Imaging. 2015 August ; 42(2): 539–544. doi:10.1002/jmri.24795.

VALIDATION OF BONE MARROW FAT QUANTIFICATION IN THE PRESENCE OF TRABECULAR BONE USING MRI

Christina S. Gee, BA[1], **Jennifer T.K. Nguyen, BA**[1], **Candice J. Marquez, BA**[1], **Julia Heunis, BA**[1], **Andrew Lai, BS**[1], **Cory Wyatt, PhD**[1], **Misung Han, PhD**[1], **Galateia Kazakia, PhD**[1], **Andrew J. Burghardt, PhD**[1], **Dimitrios C. Karampinos, PhD**[2], **Julio Carballido-Gamio, PhD**[1], and **Roland Krug, PhD**[1,*]

[1]Department of Radiology and Biomedical Imaging, University of California, San Francisco, San Francisco, CA, USA

[2]Department of Diagnostic and Interventional Radiology, Technische Universität München, Munich, Germany

Abstract

Purpose—To validate six-echo, chemical-shift based MRI with T_2* correction for the quantification of bone marrow fat content in the presence of trabecular bone.

Materials and Methods—Ten bone phantoms were made using trabecular bone cores extracted from the distal femur and proximal tibia of twenty human cadaveric knees. Bone marrow was removed from the cores and the marrow spaces were filled with water-fat gelatin to mimic bone marrow of known fat fractions. A chemical-shift based water-fat separation method with T_2* correction was employed to generate fat fraction maps. The proton density fat fractions (PDFF) between marrow regions with and without bone were compared to the reference standard of known fat fraction using the squared Pearson correlation coefficient and unpaired t-test.

Results—Strong correlations were found between the known fat fraction and measured PDFF in marrow without trabecular bone (R^2=0.99; slope=0.99, intercept=0.94) as well as in marrow with trabecular bone (R^2=0.97; slope=1.0, intercept=−3.58). Measured PDFF between regions with and without bone were not significantly different (p=0.5). However, PDFF was systematically underestimated by −3.2% fat fraction in regions containing trabecular bone.

Conclusion—Our implementation of a six-echo chemical-shift based MRI pulse sequence with T_2* correction provided an accurate means of determining fat content in bone marrow in the presence of trabecular bone.

Keywords

Fat quantification; Bone marrow fat content; Validation; 3 Tesla

*Correspondence to: Roland Krug, PhD, China Basin Landing, 185 Berry Street, Suite 350, Box 0946, San Francisco, CA 94107, phone (415) 353-4945, fax (415) 353-9423, roland.krug@ucsf.edu.

Introduction

In recent years, there has been an increasing interest in the quantification of bone marrow fat content as this might be an important and useful tool to advance our understanding of the role of bone marrow adiposity in osteoporosis (1–3). It has been found that osteoblasts and adipocytes differentiate from the same mesenchymal stem cells and that there are pathophysiologic links between bone and adipose tissue (4,5). Previous work has focused on using single-voxel MR spectroscopy (MRS) to measure fat content in localized regions, primarily within the vertebral bodies and proximal femur (2,3,6,7). The relationship between bone marrow fat content and gender (8) as well as age (9) have been reported. Furthermore, fat content has been associated with skeletal fragility and osteoporosis (10,11) suggesting that bone marrow fat composition could be a biomarker for fracture risk in postmenopausal women (12). In addition, many diseases such as diabetes mellitus (1), or Gaucher disease (13) alter the bone marrow composition. Thus, an accurate assessment of fat content in the bone marrow would be highly relevant to the field of osteoporosis.

Because the distribution of bone marrow fat content can strongly vary, particularly in the proximal femur, there is growing interest in high-resolution chemical-shift based water-fat imaging (14,15) to assess proton density fat fraction (PDFF) (16,17). Excellent agreement between PDFF and MRS has been demonstrated for a range of organs (18–21). Additionally PDFF has been successfully validated by bulk chemical analysis (22). Recent improvements of the technique account for multiple confounding factors, including main magnetic field inhomogeneity (23), the presence of multiple peaks in the fat spectrum (24,25), T_2* effects (24,26), T_1 effects (24,27,28), eddy current effects (29,30), and the presence of susceptibility-induced fat resonance shifts (31).

The presence of trabecular bone complicates fat quantification for both MRS and chemical-shift based methods. Because trabecular bone is more diamagnetic than bone marrow there is a difference in magnetic susceptibility between the two tissues that broadens the spectrum of Larmor frequencies in the presence of microscopic magnetic field inhomogeneities (32,33) leading to shorter T_2* relaxation times (34). In single-voxel MRS it broadens the linewidths of all the associated peaks, making it difficult to accurately quantify these peaks (6,7). Using water-fat imaging, the increased T_2* effect induces a rapid decay of the measured gradient echo signal with echo time (TE) (24,26). However, the value of quantitative water-fat imaging in bone marrow in the presence of trabecular bone was recently demonstrated, and excellent agreement was found with single-voxel MRS when accounting for short T_2* components potentially associated with collagen-bound water (15). The present study seeks to validate six-echo water-fat MRI with T_2* correction in bone marrow phantoms of known fat concentration with and without the presence of trabecular bone.

Materials and Methods

Phantom Preparation

Ten water-fat bone phantoms were made using trabecular bone cores extracted from the distal femur and proximal tibia of twenty human cadaveric knees. During extraction, bones

were cut using the Buehler Isomet 1000 Precision Saw (Buehler, Lake Bluff, IL, USA). Cores were removed from specimens using the Servo 7170 Drill Press (Servo Products, Eastlake, OH, USA). Cores measured 27 mm in diameter and approximately 20 mm in height. Marrow was removed from the cores first by ultrasonication in a 1% tergazyme solution using the Branson 2510 Ultrasonicator (Emerson Industrial Automation, Danbury, CT, USA) and then cleaned using gentle streams of water. Cores were cleaned until they appeared translucent and trabecular structure was visible through the depth of the cylinder. For storage, the cores were wrapped in PBS (phosphate buffer saline)-soaked gauze before being placed in a −20°C freezer.

On the day phantoms were made, the cores were removed from the freezer and placed into 50-mL centrifuge tubes (30×155-mm). To prepare bone phantoms containing different percentages of fat (by volume), homogeneous mixtures of 225 bloom beef 40 mesh gelatin, deionized water, and commercially available 100% peanut oil were produced. A mixture containing 0.1596-grams of 225 bloom gelatin (Gelatin Innovations Inc., Schiller Park, IL) per milliliter of deionized water was placed in a 121°C autoclave for thirty minutes and cooled down to 50–55°C degrees before further action. In order to ensure that the mixture remained homogeneous, 50.0 mL of 100% peanut oil (at 50–55°C) were added into the mixture in alternation with 1.0-mL of concentrated dish-washing liquid (emulsifier) for every 100.0-mL of total oil in each phantom until the solution with the proper water-fat ratio was completely mixed. Peanut oil was chosen because it has a proton NMR spectrum similar to that of triglyceride protons in adipose tissue (25). The dielectric and thermal properties of the phantom can be found in (35). All contents of the mixtures were manually mixed and placed inside a vacuum chamber for one minute to minimize the presence of air bubbles. After the addition of 10% buffered formaldehyde (4.0-mL per 100-mL of water), mixtures were immediately poured into centrifuge tubes containing the cores. The bone cores were fixed in the middle of the tubes so that the fat solution could flow through the cores filling the empty marrow spaces. As a result, each tube contained a region of fat with bone as well as a region with fat only. The range of fat fractions was from 40% to 80% simulating in-vivo conditions in the proximal femur. Ten bone scores with the highest quality were then selected for final MR imaging.

Image Acquisition and Analysis

MR imaging of the bone cores was performed on a clinical 3 T whole-body scanner (MR750, GE Healthcare, Waukesha, WI, USA) using an 8-channel transmit/receive knee coil (In-Vivo Coorporation, Gainesville, FL). A six-echo 3D spoiled gradient echo (SPGR) sequence was used for chemical-shift based water-fat separation with the following imaging parameters similar to those previously used in an in-vivo study (15): two echoes per TR, TR/TEmin/ΔTE=8/2.1/1.0 ms, FOV=20×20 cm^2, acquisition matrix=150×150, slice thickness=2 mm, and receiver bandwidth=62.5 kHz. Given the large T1 difference between water and fat components in bone marrow (36), a flip angle of 3° was used to minimize T1-bias effects. The gradient echo imaging data were reconstructed on the scanner using iterative decomposition of fat and water with echo asymmetry and least-squares estimation (IDEAL) to perform water-fat separation and to obtain the PDFF maps as well as a T_2* maps (37,38). The IDEAL algorithm (37–39) was employed with T_2* correction and a multi-peak model

for the fat spectrum (25). The IDEAL T_2* correction is performed by using a modified signal model that estimates water, fat, and T_2* simultaneously to decouple the effects of T_2* from those induced by the chemical shift of fat (25). High-resolution MR images were acquired using a fully balanced steady state (bSSFP) pulse sequence with 234 μm^2 in-plane resolution and 500 μm slice thickness (40). The pulse sequence featured a readout bandwidth of 64.5 kHz, flip angle=60°, TR=6.9 ms, and TE=2.7 ms. These images were used to assess phantom quality and to identify the bone regions. High-resolution peripheral quantitative computed tomography (HR-pQCT) images were acquired with 82 μm isotropic voxel size (XtremeCT, Scanco Medical AG, Brüttisellen, Swizterland).

Statistical Analysis

Regions of interest (ROI) were manually drawn on the PDFF maps. These ROIs consisted of simple circles containing all bone marrow. For regions containing trabecular bone, we have additionally used the high-resolution images to ensure that all bone regions were included. Mean fat-fraction values in the presence of trabecular bone were compared with mean fat fraction values obtained in the absence of trabecular bone. Both values were compared to the known fat fractions as the reference standard. The linear relationship between these values was estimated with the squared Pearson correlation coefficient (R^2), and the slope and intercept of the best-fit line. Two-sided t-tests at a significance level of p=0.05 were used to determine whether the estimated slope and intercept were statistically different from 1.0 and 0.0, respectively. A two-sided t-test was conducted between regions with bone and regions without bone to assess if the measured mean PDFF values were significantly different. In order to establish the level of agreement between these measurements Bland-Altman plots were also generated.

Results

Figure 1 shows representative HR-pQCT images of two phantoms. The left image demonstrates the feasibility of the phantom construction. It can be clearly seen that the fat occupies all marrow spaces within the trabecular bone network. As a comparison, the right figure visualized a bone core with residual air bubbles. These phantoms were discarded from the study. Figure 2 shows typical PDFF maps with and without the presence of trabecular bone. Table 1 summarizes the results of this study. The mean PDFF values along with the standard deviation are shown for regions with and without bone. As can also be seen in Figure 2b, the mean PDFF are slightly lower and the standard deviation is larger in the presence of bone.

Strong correlations with R^2=0.99; slope=0.99 (p=0.91), and intercept=0.94 (p=0.95) were found between the known fat fraction and measured PDFF in marrow (Figure 3). The comparison between known fat fraction and PDFF in the presence of trabecular bone also showed good correlation with R^2=0.97; slope=1.0 (p=0.5), and intercept=−3.58 (p=0.16). Measured PDFF between regions containing only bone marrow and regions with both bone marrow and trabecular bone were not significantly different (p=0.5). A strong and significant (p<0.001) correlation between both PDFF measurements was found with a squared Pearson correlation coefficient of R^2=0.96, and a best-fit line slope and intercept of

1.0 and −3.8 respectively (Figure 3). All estimated slopes were not significantly different from 1 ($p>0.05$) and all estimated intercepts were not significantly different from 0 ($p>0.05$).

The Bland Altman plot of the data shown in Figure 4 illustrates the differences between the PDFF measurements and the known fat fractions. Following the Bland Altman nomenclature (41), the mean difference d along with the ±1.96 standard deviation was reported. Assuming a normal distribution, 95% of PDFF differences lie between 1.95 times the standard deviation. An excellent agreement between PDFF in marrow and the reference standard is shown in Figure 4a with a mean difference of d=0.4% ± 2.6% fat fraction. Figure 4b depicts the differences between PDFF in the presence of trabecular bone and the known fat fraction. An underestimation of d=−3.2% ± 3.8% fat fraction of the measured PDFF compared to the known fat fraction is clearly demonstrated. Comparing the two measured PDFF with and without trabecular bone, a mean difference of d=−3.6%±4.5% PDFF was determined again indicating that the PDFF in the presence of trabecular bone is slightly underestimated. The T_2* values were very similar for all bone cores with a mean and standard deviation of 12ms ± 1ms reflecting similar bone densities (34).

Discussion

In this work, we have validated water-fat imaging using six-echoes and IDEAL reconstruction with T_2* correction in phantoms consisting of trabecular bone cores obtained from cadaveric knees embedded in water-fat gelatin with different fat concentrations. We have demonstrated that the PDFF values are very similar in fat with and without the presence of trabecular bone and that the PDFF values strongly correspond to the known fat fraction. In a previous study, the improvement of IDEAL with T_2* correction over previous non-corrected Dixon methods was demonstrated in fat phantoms with different iron concentrations (42). For this reason, we have adapted this advanced method to validate PDFF in the presence of trabecular bone. Furthermore, Hu et al (43) used the same method to validate PDFF against chemical analysis in different tissue and demonstrated that water-fat MR imaging has the ability to accurately estimate absolute fat mass. More recently, Karampinos et al. (15) showed that water-fat IDEAL highly correlates with MR spectroscopy measurements in bone marrow in the presence of trabecular bone. They showed excellent agreement of both techniques in-vivo in the proximal femur where bone marrow fat content can strongly vary. In the current study, we have now shown that PDFF values obtained from IDEAL in homogenous water-fat phantoms with and without trabecular bone do not significantly differ and thus IDEAL with T_2* correction is very robust even in the presence of trabecular bone.

The assessment of bone marrow fat content and fat changes can be very important for different musculoskeletal applications. In particular, it can serve as a marker for bone marrow healing and neoplastic bone marrow diseases (44). In healthy subjects, there is a conversion from red bone marrow to yellow bone marrow with age and thus, only around half of the adult bone marrow is red. In particular, important fractures sites such as the proximal femur and the spine still contain a significant amount of red marrow in adulthood. At the spine, the fat content is approximately 50% PDFF in healthy adults, and higher in patients with osteoporosis (10,11). At the proximal femur, the fat content typically varies

from around 40 % to 95 % PDFF, depending on the subject as well as the exact location (15). Therefore, we have manufactured fat phantoms in this range of expected PDFF values. Although we have found a very strong correlation between regions with trabecular bone and regions without bone, PDFF was systematically underestimated when bone was present independent of the actual fat content. There might be several reasons for this underestimation. First, the bone itself might have contributed to some of the water signal. However, our first echo was acquired at 1.5 ms and thus it is more unlikely that collagen-bound bone water with a ultra short T2 decay in the order of 50 μs could have contributed to the acquired signal (45). Another source of some bias could be the presence of macroscopic magnetic field inhomogeneity effects as previously described (46). Furthermore, any differences in T_2* between the water and the multiple spectral components in fat might have influenced the results. The main constituent of fatty yellow marrow as well as peanut oil is fatty acid triglyceride, which has multiple spectral components (47). The IDEAL calibration assumes the presence of six peaks and the T_2* correction assumes the same T_2* relaxation times for all the fat peaks and the water. However, it has been previously suggested that in bone marrow, different T_2 relaxation rates of the various protons in fat can cause errors in T_2* estimation (48). This effect could potentially lead to an underestimation of the fat content and might be related to the small bias found in this study. Although difficult, signal modeling allowing for independent correction of T_2* for the different fat components as well as water might be useful towards more accurately estimating fat-fraction in the presence of trabecular bone.

There are other potential limitations of our study. The manufacturing process of the fat phantoms with bone cores is extremely challenging and involved several critical steps. Although great care was taken to remove all the bone marrow and replace it by fat, this was very difficult for some denser bone specimens and as a consequence many of these cores were not included in the study. However, residual bone marrow may have persisted in some of the pore spaces. Furthermore, filling the empty marrow spaces with fat solution was equally challenging. Although Figure 1a demonstrates the feasibility, small non-visible air bubbles and small spatial variations of the fat distribution might have impacted our results. However, in regions without bone, the standard deviation of measured PDFF was between 1% and 2% PDFF demonstrating a homogenous fat distribution.

In summary, in this work we have demonstrated that water-fat imaging with T_2* correction can accurately assess bone marrow fat content in the presence of trabecular bone. This is a necessary step towards clinical studies investigating the relationship of bone marrow fat content and its spatial distribution in varies patient groups.

Acknowledgments

Grant Sponsors: This work was supported by NIH/NIAMS R01AR057336

References

1. Baum T, Yap SP, Karampinos DC, et al. Does vertebral bone marrow fat content correlate with abdominal adipose tissue, lumbar spine bone mineral density, and blood biomarkers in women with type 2 diabetes mellitus? J Magn Reson Imaging. 2012; 35(1):117–124. [PubMed: 22190287]

2. Griffith JF, Yeung DKW, Antonio GE, et al. Vertebral bone mineral density, marrow perfusion, and fat content in healthy men and men with osteoporosis: dynamic contrast-enhanced MR imaging and MR spectroscopy. Radiology. 2005; 236(3):945–951. [PubMed: 16055699]
3. Griffith JF, Yeung DKW, Antonio GE, et al. Vertebral marrow fat content and diffusion and perfusion indexes in women with varying bone density: MR evaluation. Radiology. 2006; 241(3): 831–838. [PubMed: 17053202]
4. Rosen CJ, Bouxsein ML. Mechanisms of disease: is osteoporosis the obesity of bone? Nature clinical practice Rheumatology. 2006; 2(1):35–43.
5. Lecka-Czernik B. Marrow fat metabolism is linked to the systemic energy metabolism. Bone. 2012; 50(2):534–539. [PubMed: 21757043]
6. Li X, Kuo D, Schafer AL, et al. Quantification of vertebral bone marrow fat content using 3 Tesla MR spectroscopy: reproducibility, vertebral variation, and applications in osteoporosis. J Magn Reson Imaging. 2011; 33(4):974–979. [PubMed: 21448966]
7. Schick F, Bongers H, Jung WI, Skalej M, Lutz O, Claussen CD. Volume-selective proton MRS in vertebral bodies. Magn Reson Med. 1992; 26(2):207–217. [PubMed: 1513248]
8. Griffith JF, Yeung DK, Antonio GE, et al. Vertebral marrow fat content and diffusion and perfusion indexes in women with varying bone density: MR evaluation. Radiology. 2006; 241(3):831–838. [PubMed: 17053202]
9. Schellinger D, Lin CS, Fertikh D, et al. Normal lumbar vertebrae: anatomic, age, and sex variance in subjects at proton MR spectroscopy--initial experience. Radiology. 2000; 215(3):910–916. [PubMed: 10831721]
10. Griffith JF, Yeung DK, Antonio GE, et al. Vertebral bone mineral density, marrow perfusion, and fat content in healthy men and men with osteoporosis: dynamic contrast-enhanced MR imaging and MR spectroscopy. Radiology. 2005; 236(3):945–951. [PubMed: 16055699]
11. Yeung DK, Griffith JF, Antonio GE, Lee FK, Woo J, Leung PC. Osteoporosis is associated with increased marrow fat content and decreased marrow fat unsaturation: a proton MR spectroscopy study. J Magn Reson Imaging. 2005; 22(2):279–285. [PubMed: 16028245]
12. Patsch JM, Li X, Baum T, et al. Bone marrow fat composition as a novel imaging biomarker in postmenopausal women with prevalent fragility fractures. J Bone Miner Res. 2013; 28(8):1721–1728. [PubMed: 23558967]
13. van Dussen L, Lips P, van Essen HW, Hollak CE, Bravenboer N. Heterogeneous pattern of bone disease in adult type 1 Gaucher disease: clinical and pathological correlates. Blood cells, molecules & diseases. 2014; 53(3):118–123.
14. Pichardo JC, Milner RJ, Bolch WE. MRI measurement of bone marrow cellularity for radiation dosimetry. J Nucl Med. 2011; 52(9):1482–1489. [PubMed: 21799087]
15. Karampinos DC, Melkus G, Baum T, Bauer JS, Rummeny EJ, Krug R. Bone marrow fat quantification in the presence of trabecular bone: Initial comparison between water-fat imaging and single-voxel MRS. Magn Reson Med. 2013
16. Reeder SB, Cruite I, Hamilton G, Sirlin CB. Quantitative assessment of liver fat with magnetic resonance imaging and spectroscopy. J Magn Reson Imaging. 2011; 34(4):729–749. [PubMed: 21928307]
17. Reeder SB, Hu HH, Sirlin CB. Proton density fat-fraction: A standardized MR-based biomarker of tissue fat concentration. J Magn Reson Imaging. 2012; 36:1011–1014. [PubMed: 22777847]
18. Hines CD, Frydrychowicz A, Hamilton G, et al. T(1) independent, T(2) (*) corrected chemical shift based fat-water separation with multi-peak fat spectral modeling is an accurate and precise measure of hepatic steatosis. J Magn Reson Imaging. 2011; 33(4):873–881. [PubMed: 21448952]
19. Hu HH, Kim HW, Nayak KS, Goran MI. Comparison of fat-water MRI and single-voxel MRS in the assessment of hepatic and pancreatic fat fractions in humans. Obesity (Silver Spring). 2010; 18:841–847. [PubMed: 19834463]
20. Meisamy S, Hines CD, Hamilton G, et al. Quantification of hepatic steatosis with T1-independent, T2*-corrected MR imaging with spectral modeling of fat: blinded comparison with MR spectroscopy. Radiology. 2011; 258:767–775. [PubMed: 21248233]
21. Yokoo T, Shiehmorteza M, Hamilton G, et al. Estimation of hepatic proton-density fat fraction by using MR imaging at 3.0 T. Radiology. 2011; 258(3):749–759. [PubMed: 21212366]

22. Hu HH, Nagy TR, Goran MI, Nayak KS. Quantification of absolute fat mass by magnetic resonance imaging: a validation study against chemical analysis. International Journal of Body Composition Research. 2011; 9(3):111–122. [PubMed: 23204926]
23. Hernando D, Haldar JP, Sutton BP, Ma J, Kellman P, Liang ZP. Joint estimation of water/fat images and field inhomogeneity map. Magn Reson Med. 2008; 59(3):571–580. [PubMed: 18306409]
24. Bydder M, Yokoo T, Hamilton G, et al. Relaxation effects in the quantification of fat using gradient echo imaging. Magn Reson Imaging. 2008; 26(3):347–359. [PubMed: 18093781]
25. Yu H, Shimakawa A, McKenzie CA, Brodsky E, Brittain JH, Reeder SB. Multiecho water-fat separation and simultaneous R2* estimation with multifrequency fat spectrum modeling. Magn Reson Med. 2008; 60(5):1122–1134. [PubMed: 18956464]
26. Yu H, McKenzie CA, Shimakawa A, et al. Multiecho reconstruction for simultaneous water-fat decomposition and T_2* estimation. J Magn Reson Imaging. 2007; 26(4):1153–1161. [PubMed: 17896369]
27. Karampinos DC, Yu H, Shimakawa A, Link TM, Majumdar S. T1-corrected fat quantification using chemical shift-based water/fat separation: application to skeletal muscle. Magn Reson Med. 2011; 66:1312–1326. [PubMed: 21452279]
28. Liu CY, McKenzie CA, Yu H, Brittain JH, Reeder SB. Fat quantification with IDEAL gradient echo imaging: correction of bias from T_1 and noise. Magn Reson Med. 2007; 58(2):354–364. [PubMed: 17654578]
29. Hernando D, Hines CD, Yu H, Reeder SB. Addressing phase errors in fat-water imaging using a mixed magnitude/complex fitting method. Magn Reson Med. 2012; 67:638–644. [PubMed: 21713978]
30. Yu H, Shimakawa A, Hines CDG, et al. Combination of complex-based and magnitude-based multiecho water-fat separation for accurate quantification on fat-fraction. Magn Reson Med. 2011; 66:199–206. [PubMed: 21695724]
31. Karampinos DC, Yu H, Shimakawa A, Link TM, Majumdar S. Chemical shift-based water/fat separation in the presence of susceptibility-induced fat resonance shift. Magn Reson Med. 2012; 68(5):1495–1505. [PubMed: 22247024]
32. Majumdar S. Quantitative study of the susceptibility difference between trabecular bone and bone marrow: computer simulations. Magn Reson Med. 1991; 22(1):101–110. [PubMed: 1798385]
33. Majumdar S, Thomasson D, Shimakawa A, Genant HK. Quantitation of the susceptibility difference between trabecular bone and bone marrow: experimental studies. Magn Reson Med. 1991; 22(1):111–127. [PubMed: 1798386]
34. Majumdar S, Genant HK. In vivo relationship between marrow T2* and trabecular bone density determined with a chemical shift-selective asymmetric spin-echo sequence. J Magn Reson Imaging. 1992; 2(2):209–219. [PubMed: 1562773]
35. Yuan Y, Wyatt C, Maccarini P, et al. A heterogeneous human tissue mimicking phantom for RF heating and MRI thermal monitoring verification. Phys Med Biol. 2012; 57(7):2021–2037. [PubMed: 22430012]
36. Schick, F.; Bongers, H.; Jung, WI., et al. Appl MagnReson. Vol. 3. Springer-Verlag; 1992. Proton relaxation times in human red bone marrow by volume selective magnetic resonance spectroscopy; p. 947-963.
37. Reeder SB, Pineda AR, Wen Z, et al. Iterative decomposition of water and fat with echo asymmetry and least-squares estimation (IDEAL): application with fast spin-echo imaging. Magn Reson Med. 2005; 54(3):636–644. [PubMed: 16092103]
38. Reeder SB, Wen Z, Yu H, et al. Multicoil Dixon chemical species separation with an iterative least-squares estimation method. Magn Reson Med. 2004; 51(1):35–45. [PubMed: 14705043]
39. Yu H, Reeder SB, Shimakawa A, Brittain JH, Pelc NJ. Field map estimation with a region growing scheme for iterative 3-point water-fat decomposition. Magn Reson Med. 2005; 54(4):1032–1039. [PubMed: 16142718]
40. Krug R, Burghardt AJ, Majumdar S, Link TM. High-resolution imaging techniques for the assessment of osteoporosis. Radiol Clin North Am. 2010; 48(3):601–621. [PubMed: 20609895]

41. Bland JM, Altman DG. Statistical methods for assessing agreement between two methods of clinical measurement. Lancet. 1986; 1(8476):307–310. [PubMed: 2868172]
42. Hines CD, Yu H, Shimakawa A, McKenzie CA, Brittain JH, Reeder SB. T1 independent, T2* corrected MRI with accurate spectral modeling for quantification of fat: validation in a fat-water-SPIO phantom. J Magn Reson Imaging. 2009; 30(5):1215–1222. [PubMed: 19856457]
43. Hu HH, Nagy TR, Goran MI, Nayak KS. Quantification of absolute fat mass by magnetic resonance imaging: a validation study against chemical analysis. International Journal of Body Composition Research. 2011; 9(3):111–122. [PubMed: 23204926]
44. Swartz PG, Roberts CC. Radiological reasoning: bone marrow changes on MRI. AJR Am J Roentgenol. 2009; 193(3 Suppl):S1–S4. Quiz S5–9. [PubMed: 19696238]
45. Gatehouse PD, Bydder GM. Magnetic resonance imaging of short T2 components in tissue. Clin Radiol. 2003; 58(1):1–19. [PubMed: 12565203]
46. Hernando D, Vigen KK, Shimakawa A, Reeder SB. R(2) mapping in the presence of macroscopic B(0) field variations. Magn Reson Med. 2012; 68(3):830–840. [PubMed: 22161866]
47. Wehrli FW, Perkins TG, Shimakawa A, Roberts F. Chemical shift-induced amplitude modulations in images obtained with gradient refocusing. Magn Reson Imaging. 1987; 5(2):157–158. [PubMed: 3586882]
48. Ma J, Wehrli FW. Method for image-based measurement of the reversible and irreversible contribution to the transverse-relaxation rate. J Magn Reson B. 1996; 111(1):61–69. [PubMed: 8620286]

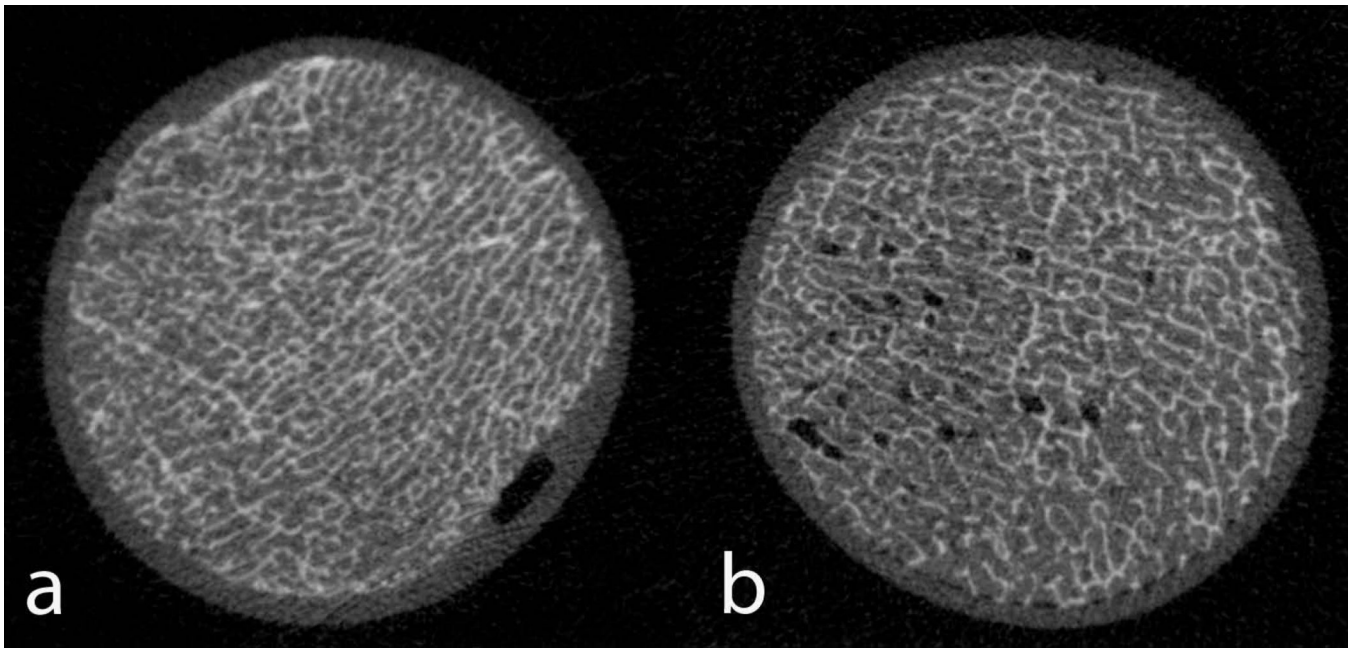

Figure 1.

Representative high-resolution HR-pQCT images of two phantoms acquired with isotropic voxel size of 82 μm. Left: It is clearly demonstrated that the fat solution nicely fills all the bone marrow spaces. Right: For comparison a bone core is shown with residual air. These air bubbles can be easily identified and these phantoms can be discarded.

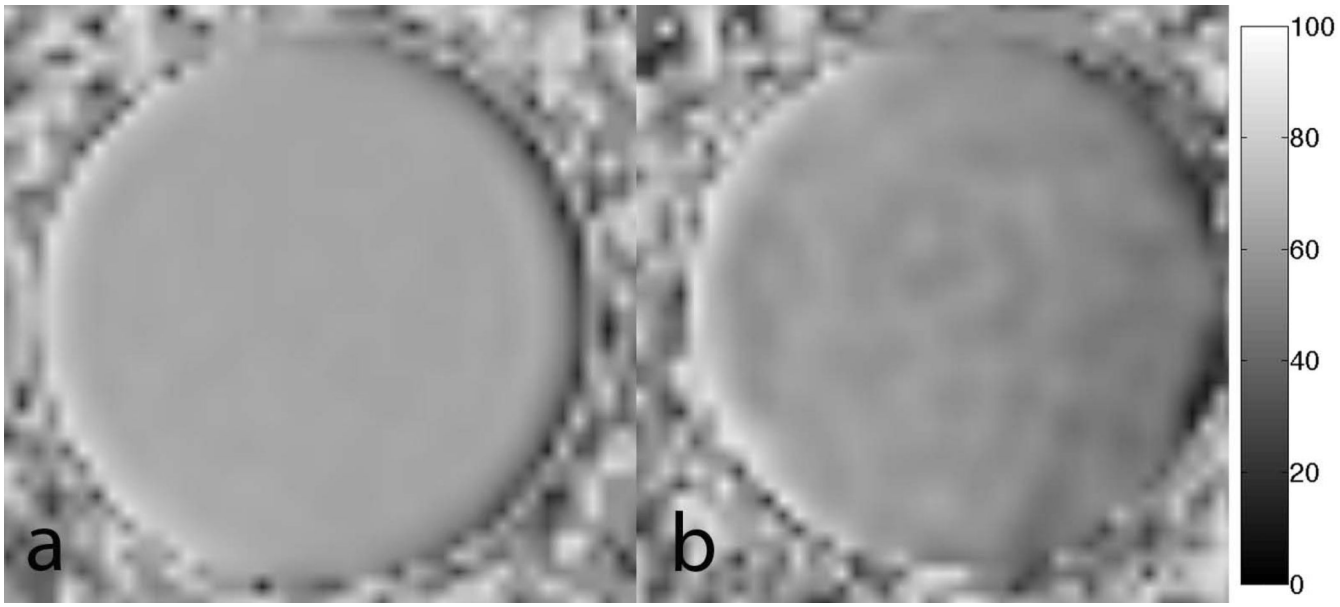

Figure 2.

Shown are the obtained IDEAL fat fraction maps. The left images show fat only in the phantom and the right images contain a bone core embedded in fat. The color bar indicates PDFF in percent fat.

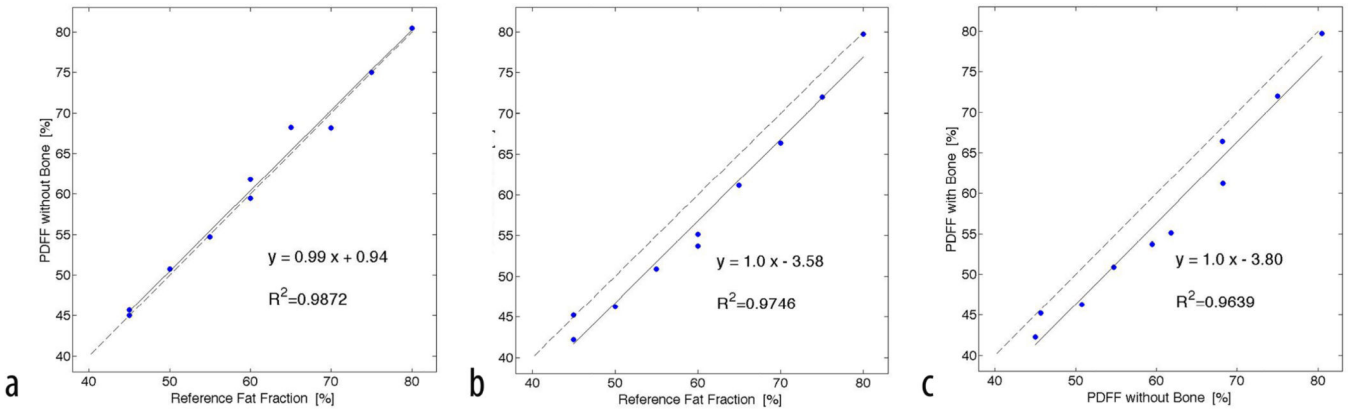

Figure 3.

Shown are the linear relationships between Standard Reference of fat fraction and PDFF in the presence of trabecular bone and without bone. a) Comparing PDFF without bone to the known fat fraction; b) Comparing PDFF with bone to the known fat fraction; c) Comparing measured PDFF with and without bone. The solid line represents the fitting results from linear regression analyses. The dashed line represents the unity line.

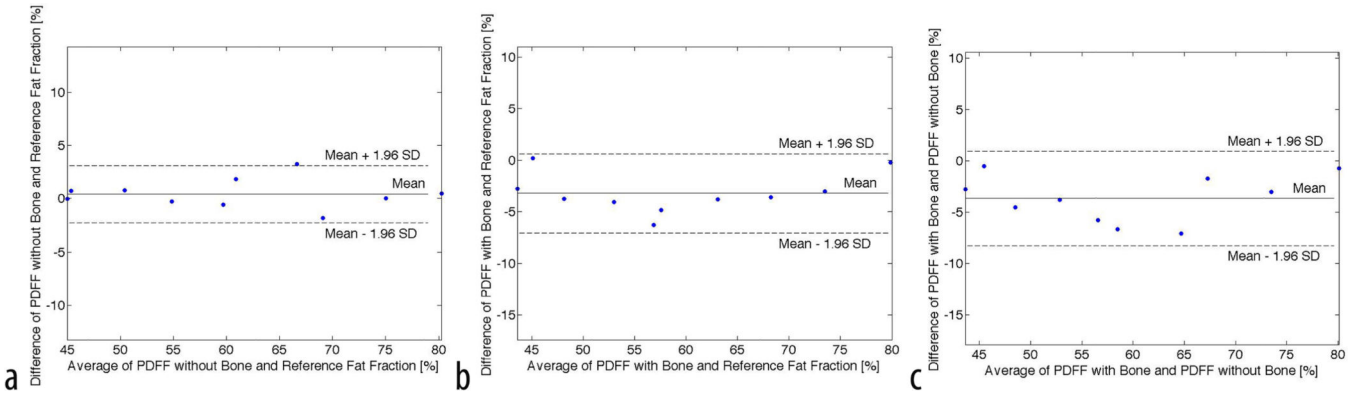

Figure 4.

Shown is the Bland-Altman plot comparing the measured PDFF fat fractions with the known fat fractions. a) Comparing differences between PDFF without bone and known fat fraction; b) Comparing differences of PDFF with bone and known fat fraction; c) Comparing PDFF with and without bone. A systematic underestimation of PDFF in the presence of bone compared to PDFF without bone and known fat fraction is clearly demonstrated.

Table 1

Shown are the Means and StdDev of PDFF in each phantom as measured by IDEAL.

	Reference Standard [%]	with Bone Mean [%]	Std Dev	without Bone Mean [%]	Std Dev
Phantom 1	80	79.78	2.68	80.49	1.18
Phantom 2	75	71.97	2.17	75.03	1.34
Phantom 3	70	66.40	2.10	68.16	1.47
Phantom 4	65	61.17	3.19	68.24	1.64
Phantom 5	60	55.13	4.41	61.80	1.82
Phantom 6	60	53.68	4.00	59.44	1.21
Phantom 7	55	50.91	3.07	54.73	2.07
Phantom 8	50	46.24	3.37	50.79	1.40
Phantom 9	45	45.21	1.92	45.70	1.02
Phantom 10	45	42.23	3.76	44.99	1.02